Available online at www.sciencedirect.com

Chemical Engineering Research and Design

journal homepage: www.elsevier.com/locate/cherd

Hybrid modeling and operating optimization method of oxidation process of wet flue gas desulfurization (WFGD) system

Zhongyang Zhao[a], *Haidong Fan*[a], *Qinwu Li*[a], *Chang Liu*[a], *Zhu Chen*[a], *Lianming Li*[b], *Chenghang Zheng*[a,c,*], *Xiang Gao*[a,c]

[a] *State Key Laboratory of Clean Energy Utilization, State Environmental Protection Center for Coal-Fired Air Pollution Control, Zhejiang University, Hangzhou 310027, China*
[b] *Jiaxing Xinjia'aisi Thermal Power Co., Ltd., Jiaxing 314000, China*
[c] *Jiaxing Research Institute, Zhejiang University, Jaixing 314000, China*

ARTICLE INFO

Article history:
Received 17 July 2022
Received in revised form
12 September 2022
Accepted 22 September 2022
Available online 26 September 2022

Keywords:
WFGD
Oxidation subsystem
Operating optimization
Hybrid model
Application

ABSTRACT

Wet flue gas desulfurization systems (WFGD) are the most popular method to remove the SO_2 from the flue gas in China's power plants. Most WFGD systems contain an oxidation subsystem, which is one of the most important subsystems. In this paper, a hybrid modeling and operating optimization method of oxidation process of WFGD system is proposed, verified and applied on the WFGD system of a typical 1000 MW unit. The influence of important parameters such as the diameter of droplets or bubbles, the liquid-gas ratio or the gas-gas ratio (the ratio of between oxidized air flow rate and flue gas flow rate) and the height of the natural oxidation zone or the slurry level on natural oxidation rate and forced oxidation rate are further explored. The application results show that the above method can significantly reduce the operating energy consumption of the oxidation fan by more than 25 %. Furthermore, field tests are also carried out on the WFGD systems of 130 t/h and 220 t/h circulating fluidized bed (CFB) units. The energy consumption can be reduced by 30.6 % and 37.5 %, respectively. The results will be helpful to reduce the auxiliary power consumption and additional CO_2 emission of WFGD.

1. Introduction

Sulfur dioxide (SO_2) plays an important role in the air pollution (Shen et al., 2019; H. Wang et al., 2019; Zheng et al., 2019), which is mainly formed during the industrial processes (Smith et al., 2011; Chang et al., 2019). The major sources of SO_2 emissions are the power generation industry (Flagiello et al., 2018; Zheng et al., 2014) and iron and steel smelting industry (X. Wang et al., 2019). In 2020, China's steel and iron smelting industry and power generation industry emitted 415 kt and 374 kt of SO_2 (China, 2021), account for 13.5 % and 11.8 % of total SO_2 emissions in China, respectively (China, 2022). In order to reduce the emission of SO_2, China's government has issued the strictest specifications worldwide (Flagiello et al., 2018; Abel et al., 2019) that the SO_2 concentration of the flue gas emitted from coal-fired power plants and ironworks should be less than 35 mg/m^3 (National Development and Reform Commission of PRC and National Energy Administration of PRC, 2014; Gu et al., 2020).

For the effective removal of SO_2, most of coal-fired power plants have adopted flue gas desulfurization (FGD) devices in China (Córdoba, 2015; Srivastava et al., 2001; Chen et al., 2020; Liu et al., 2022). And, wet flue gas desulfurization (WFGD) system is one of the most favorite technologies due to its unique characteristics such as high efficiency, and reliability (Zheng et al., 2019; Gong and Yang, 2018; Zou et al., 2020;

* Correspondence to: State Key Lab of Clean Energy Utilization, State Environmental Protection Center for Coal-Fired Air Pollution Control, Zhejiang University, Hangzhou 310027, China.
E-mail address: zhengch2003@zju.edu.cn (C. Zheng).

https://doi.org/10.1016/j.cherd.2022.09.045
0263-8762/

Nomenclature

a	interfacial area, m^2.
a'	gas-liquid specific surface area, m^2/m^3.
c_1, c_2	learning factors.
c_{O_2}	concentration of O_2, mol/m^3.
$c_{S(IV)}$	calculated concentration of sulfite, mol/m^3.
$\hat{c}_{S(IV)}$	measured concentration of sulfite, mol/m^3.
c_{SO_2}	concentration of SO_2, mg/m^3.
C_D	drag coefficient.
D_d	diameter of droplet, m.
$D_{b,t}$	diameter of bubble at time t, m.
D_t	diameter of absorber, m.
D_{g,O_2}	molecular diffusivity of O_2 in gas phase, m^2/s.
D_{l,O_2}	molecular diffusivity of O_2 in liquid phase, m^2/s.
E	enhancement factor.
E_n	enhancement factor of natural oxidation process.
E_f	enhancement factor of forced oxidation process.
g	gravitational acceleration, N/kg.
h	height between the bubble and the slurry plane, m.
H_{O_2}	Henry's constant of O_2, $Pa\,mol^{-1}\,m^3$.
H_f	height of forced oxidation zone, m.
H_n	height of natural oxidation zone tank, m.
H_s	slurry level of in the slurry tank, m.
k_g	gas phase mass transfer coefficient, mol/(m^2 s Pa).
k_l	liquid phase mass transfer coefficient, m/s.
K_g	gas phase mass transfer coefficient, mol/(m^2 s Pa).
K_1, K_2	correlation factors.
l_e	Kolmogorov length, m.
L	flow rate of liquid, m^3/s.
M_{air}	molecular weight of air, g/mol.
M_{O_2}	molecular weight of O_2, g/mol.
M_{SO_2}	molecular weight of SO_2, g/mol.
$n_{i,t}$	mole of the ith gas component at time t, mol.
N_{O_2}	mass transfer flux of O_2, mol/(m^2 s).
P	pressure, Pa.
P_{atm}	atmospheric pressure, Pa.
$P_{b,t}$	pressure inside the bubble at time t, Pa.
P_{gbest}	best position of the whole particle swarm.
$P_{i,t}$	position of particle i in iteration t.
p_{O_2}	partial pressure of O_2, Pa.
$P_{pbest,i}$	best position of particle i.
Q_a	oxidize air flow rate, m^3/s.
Q_f	flue gas flow rate, m^3/s.
r_1, r_2	random numbers ranging from 0 to 1.
R	universal gas constant, 8.3141 J/(mol K).
Re_g	Reynold number of gas phase.
Re_l	Reynold number of liquid phase.
r_{ox}	oxidation rate of sulfite.
S	cross-sectional area of the slurry tank, m^2.
S_{ab}	absorbed sulfur during a period of time, mol.
S_{ox}	oxidated sulfur during a period of time, mol.
Sc	Schmidt number.
Sh	Sherwood number.
t	time, s.
T	temperature, K.
$u_{b,t}$	velocity of gas at time t, m/s.
u_d	velocity of droplet, m/s.
u_e	Kolmogorov velocity, m/s.
u_r	relative velocity between gas and liquid, m/s.
υ_l	kinematic viscosity of liquid, m^2/s.
υ_m	mole volume of gas, m^3/mol.
V_{air}	molecule diffusion volume of air, cm^3/mol.
$V_{i,t}$	velocity of particle.
V_{O_2}	molecule diffusion volume of O_2, cm^3/mol.
x	number of measured values.
X	number of gas components.

Greek letters

ω	inertia weight.
ε	turbulent energy dissipation, m^2/s^3.
ε_m	modified turbulent energy dissipation, m^2/s^3.
ρ_g	density of gas, kg/m^3.
ρ_l	density of liquid, kg/m^3.
μ_g	viscosity of gas, Pa/s.
μ_l	viscosity of liquid, Pa/s.
σ	Surface tension, N.
κ	μ_g/μ_l, viscosity ratio.
η_1	natural oxidation rate.
η_2	utilization rate of oxidize air.
η_{SO_2}	desulfurization efficiency.
Φ_{O_2}	mole fraction of O_2 in the air.

Kallinikos et al., 2010). The most commonly used absorbent of WFGD system is limestone because its wide range of sources and low cost. The SO_2 in the flue gas is absorbed by the slurry of limestone in the absorber of WFGD system. And, the oxidation of sulfite is one of the important intermediate reactions in the WFGD.

In recent decades, many researchers have conducted in-depth research on the oxidation mechanism of sulfite. Jia et al. (2010) used bubbling apparatus to investigate the kinetics of oxidation of total sulfite in ammonia-based WFGD process and built a kinetic model according to the experimental results. Guo et al. (2017) investigated the kinetics of jet aeration oxidation of magnesium sulfite. The results showed the oxidation reaction rate was 0.62 order in sulfite ion and zero-order in oxygen. Shen et al. (2012) carried out an experiment in a stirred bubbling reactor to investigate the kinetics of sulfite oxidation in the magnesium-based WFGD process. The oxidation reaction was found to be 0.88 order with the concentration of magnesium sulfite and mainly controlled by the O_2 diffusion. Similarly, Chen et al. (2017) made a conclusion that the oxidation rate of sulfite is mainly controlled by the mass transfer of O_2 due to the rapid chemical reaction, after carried out the experiment using bubbling apparatus. Liu et al. (2017) presented a method to predict the oxidation efficiency of $MgSO_3$ oxidation reaction in aeration tank with computational fluid dynamics (CFD) software. The multi-phase flow field model was set up using the multi-fluid model and dispersive k-ε model. The model is reliable compared with the results of the actual ship test. Zhang et al. (2016) put forward a micro-pore aeration system to study the effects of key factors such as pH and temperature, and built a model to predict the oxidation performance at different condition with artificial neutral network (ANN).

The oxidation of sulfite in the absorber is very important for the safe operation of the WFGD system (Yi et al., 2011). Experience shows that if the oxidation rate is maintained within a certain range (generally between 0.15 and 0.3)

(Srivastava and Jozewicz, 2001), the problem of scale formation is most likely to happen. Thus, after developed and utilized over a century, the WFGD technology gradually divided into two different types (Pyshyev et al., 2017). One is the "inhibited-oxidation" type, to keep the system oxidation fraction below 0.15. The by-product is mainly calcium sulfate or calcium sulfate hemihydrate. The other is the "forced-oxidation" type, to keep the oxidation fraction above 0.95. The by-product is mainly gypsum. Actually, the choice between the two process options depends primarily on the methods feasible for byproduct solids disposal (Pandey et al., 2005). At present, most of all the coal-fired power plants in China have adopted forced-oxidation type WFGD systems.

The oxidation subsystem is one of the most important subsystems in the forced-oxidation type WFGD systems, which is also an important part of the energy consumption of WFGD system (Li et al., 2022). Considering the wide range of inlet SO_2 concentration and flue gas flow rate caused by the fluctuation of load and coal properties, the oxidation subsystems are commonly designed with a large operation margin to guarantee the oxidation rate, resulting in high auxiliary power consumption and additional CO_2 emission. In order to enhance the economic performance of WFGD, several researches in recent years have been devoted to the optimal operation of the oxidation subsystem in WFGD. Ma et al. (2019) put forward a optimization method of the oxidation process by an oxidation reduction potential (ORP) control strategy. The OPR is timely measured by an online ORP meter, which can accurately reflect the slurry condition in the absorber. The absorber can be operated in optimum conditions and realize the goal of oxidation control accurately in the slurry oxidation by stages based on the system. The results provide theoretical guidance for precise oxidation control of the WFGD slurry system.

As mentioned above, there are numbers of works devoted to study the oxidation mechanism of sulfite. These existing researches have made many detailed studies on the mechanism of oxidation. However, such researches are mainly at the laboratory level and focus on the oxidation reaction in the slurry tank. There are few studies focus on modeling the oxidation process including both nature oxidation and forced oxidation in an actual absorber. In fact, due to the different design and operating conditions, it is difficult to build a general and accurate mechanism model. At the same time, the online ORP meter is needed in the above-mentioned research on the operating optimization of the oxidation system, which will bring the additional cost. It is important to develop an optimization method based on the existing equipment in the plant.

Therefore, in this paper, a hybrid modeling and operating optimization method of oxidation process of WFGD system is proposed, verified and applied on the WFGD system of a typical 1000 MW unit. The influence of important parameters such as the diameter of droplets or bubbles, the liquid-gas ratio or the gas-gas ratio (the ratio of between oxidized air flow rate and flue gas flow rate) and the height of the natural oxidation zone or the slurry level on natural oxidation rate and forced oxidation rate are further explored. The application results show that the above method can significantly reduce the operating energy consumption of the oxidation fan by more than 25 %. Furthermore, field tests are also carried out on the WFGD systems of 130 t/h and 220 t/h circulating fluidized bed (CFB) units. The energy consumption can be reduced by 30.6 % and 37.5 %, respectively. The results will be helpful to reduce the auxiliary power consumption and additional CO_2 emission of WFGD.

2. Methodology

2.1. *Process description*

The oxidation process in a typical WFGD absorber is shown in Fig. 1. The oxidation process of sulfite in the absorber involves natural oxidation process and forced oxidation process. The sulfite in the droplets will be oxidized by the oxygen in the flue gas during the falling process of droplets, which is called natural oxidation process. Besides, the sulfite in the slurry tank will be oxidized by the oxidize air from the oxidation fan, which is called forced oxidation process. Whatever where the oxidation process occurs, the main

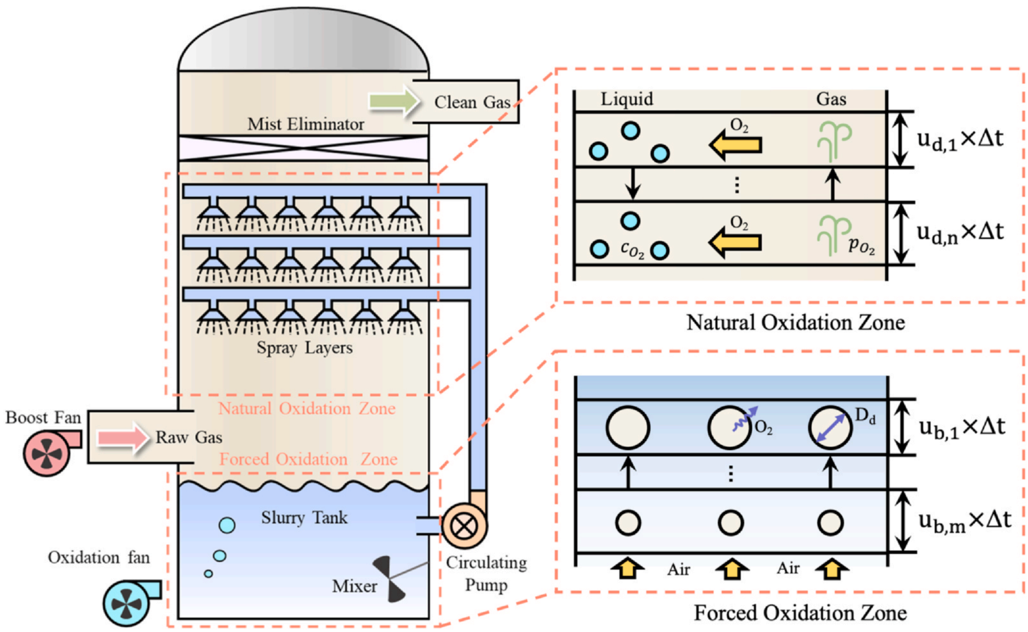

Fig. 1 – Diagrammatic sketch of oxidation process in a typical WFGD absorber.

reactions are the same and can be divided into four parts by the characteristics of each reaction:

(1) The absorption of O_2:

$O_2(g) \leftrightarrow O_2(aq)$

(2) The dissolution of $CaSO_3$:

$Ca^{2+} + SO_3^{2-} \leftrightarrow CaSO_3$

(3) The ionization equilibrium:

$SO_2(aq) + H_2O \leftrightarrow HSO_3^- + H^+$

$HSO_3^- \leftrightarrow SO_3^{2-} + H^+$

$H_2O \leftrightarrow H^+ + OH^-$

(4) The oxidation of S(IV):

$HSO_3^- + 1/2O_2 \rightarrow H^+ + SO_4^{2-}$

$SO_3^{2-} + 1/2O_2 \rightarrow SO_4^{2-}$

2.2. *Model development*

As mentioned above, the aim of our work in this paper is to develop an optimization method of the oxidation process based on the existing equipment. And the most important part is to model the oxidation process of the WFGD system. Because of the high requirement of safety by large coal-fired power plants, a reliable model is needed for operating optimization of the oxidation process. The model is supposed to be accurate, interpretable and robust. Although the data-driven model has known a great success in recent years which can make accurate predictions or classifications, its interpretability and the robustness are difficult to meet the application requirements (Guo et al., 2019). Thus, an interpretable and robust mechanism-based model is appropriate to describe the oxidation process. Our previous work has already built a mechanism-based model of the oxidation process (Liu et al., 2021). The mechanism-based model has obtained good verification results in the laboratory. However, because of the complex condition in the full-scale WFGD system, some parameters are difficult to be measured and therefore require a large number of assumptions (Guo et al., 2018), which limit the accuracy of the mechanism-based model. As a result, a hybrid modeling method is purposed. The model is mainly based on the mechanism of the oxidation process in the WFGD, and the key factors are identified by the particle swarm optimization (PSO) algorithm, which lead to the better accuracy, interpretability and robustness of the hybrid model.

2.2.1. *Assumptions*

The main purpose of the mechanism model is to ensure that the calculation results are always in line with common sense. In order to ensure the rapidity of calculation, some assumptions can be used to simplify the calculation process. The oxidation process in the absorber is a complex process, and is difficult to be fully and accurately described only by mathematical methods (Zhou et al., 2017). As a result, it is necessary to simplify the model with several appropriate assumptions. These assumptions ignore the effect of some phenomena on the oxidation process in the absorber, but will not affect the overall trend of the effect of key parameters on the natural or forced oxidation rate, which will not only reduce the complexity of the mathematical model, but also greatly increase the computational speed. Therefore, the following assumptions are made for the model:

1. The droplets and bubbles are considered to be a standard sphere. All droplets and bubbles are evenly distributed on the horizontal plane. There is no collision between droplets and between and bubbles.
2. The flue gas and oxidize air are regarded as the ideal gas. The slurry in the slurry tank is fully mixed.
3. The flow rate of flue gas is not affected by mass transfer. The natural oxidation process is believed to be controlled by the mass transfer of O_2.

It is worth noting that during the natural oxidation process, the droplets and the flue gas are in countercurrent contact. The common method to solve the countercurrent absorption problem is bisection method (Zhao et al., 2022, 2021). However, the bisection method will significantly increase the amount of computation, which can be avoided by Assumption 3. In fact, there are already some studies that justify Assumption 3, such as the work of Shen et al. (2012), Chen et al. (2017) and our previous work (Liu et al., 2021).

2.2.2. *Mass transfer and reaction in the oxidation process*

The mass transfer and reaction during the oxidation process is shown in Fig. 2. In the nature oxidation zone, the O_2 in the flue gas is absorbed by the droplet while in the forced oxidation zone, the O_2 in the oxidize air is absorbed by the slurry in the slurry tank. The mass transfer process can be described by the following equation, and the Henry's constant of can be obtained according to the works of Sander (2015):

$$N_{O_2} = K_g(p_{O_2} - H_{O_2}c_{O_2}) \tag{1}$$

The total mass transfer coefficient can be obtained by:

$$\frac{1}{K_g} = \frac{1}{k_g} + \frac{H_{O_2}}{k_l \cdot E} \tag{2}$$

According to the FrÖssling correlation (Gerbec et al., 1995), the gas phase mass transfer coefficient can be obtained by:

$$Sh = \frac{k_g dRT}{D_{O_2}} = 2 + 0.55Re_g^{0.5}Sc^{\frac{1}{3}} \tag{3}$$

The gas diffusion coefficient, representing the diffusion capacity of gas (Lee, 2000), can be obtained by FSG method, expressed by Fuller et al. (1966), and the mole volume and the

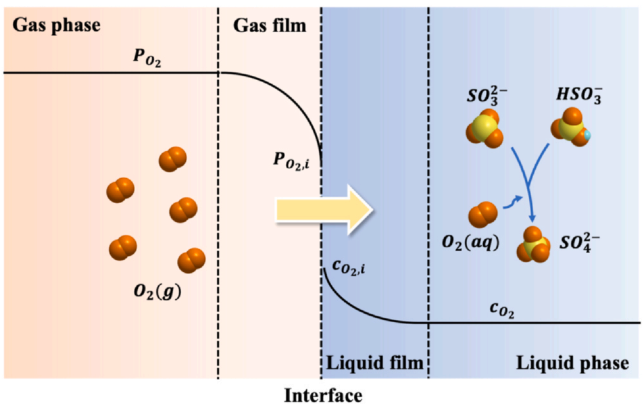

Fig. 2 – Mass transfer and reaction in the oxidation process.

molecular weight can be find in the same paper as mentioned above:

$$D_{O_2} = \frac{9.86 \times 10^{-9} \cdot T^{1.75} \cdot \left[\frac{1}{M_{air}} + \frac{1}{M_{O_2}}\right]^{\frac{1}{2}}}{0.000001 \cdot p \cdot (v_{air}^{\frac{1}{3}} + v_{O_2}^{\frac{1}{3}})^2} \tag{4}$$

The liquid mass transfer coefficient can be obtained according to the works of Banerjee et al. (1968):

$$k_l = \sqrt{\frac{D_{l,SO_2} u_e}{l_e}} \tag{5}$$

Based on the first similarity hypothesis of Kolmogorov (Lawson et al., 2019), the l_e and u_e can be determined by the viscous dissipation of energy per unit mass (ε_m) and the kinematic viscosity (v):

$$l_e = \left(\frac{v^3}{\varepsilon_m}\right)^{\frac{1}{4}} \tag{6}$$

$$u_e = (v\varepsilon_m)^{\frac{1}{4}} \tag{7}$$

D_l can be obtained according to the work of Othmer and Thakar (1953), as shown in Eq. (8):

$$D_{l,O_2} = \frac{1.4 \times 10^{-8}}{V_{O_2}^{0.6} \mu_l^{1.1}} \tag{8}$$

High velocity convection occurs between the droplet (or bubble) and the surrounding fluid, which causes surface fluctuations. At a low velocity, liquid surface is impacted by the eddies, resulting in deformations controlled by surface tension. For sufficiently small eddies, the energy of the eddies balances the surface tension acting on the surface deformation. Therefore, the modified turbulent energy dissipation can be expressed as:

$$\varepsilon_m = \varepsilon - \frac{\sigma da + a d\sigma}{m dt} \tag{9}$$

where, ε can be determined by Eq. (10) (Lamont and Scott, 1970):

$$\varepsilon = 1.6 \times 10^{-13} Re_l^{2.75} v_l^3 / d^4 \tag{10}$$

2.2.3. *Motion of droplets in nature oxidation process*

The motion of droplets in the nature oxidation zone is obtained can be described by the balance of forces acting (Michalski, 2000) which can be shown as followed:

$$\frac{\pi}{6} D_d^3 \rho_l \frac{du_d}{dt} = \frac{\pi}{6} D_d^3 (\rho_l - \rho_g) g - C_D \rho_g \frac{\pi}{4} D_d^2 \frac{u_r^2}{2} \tag{11}$$

where the drag coefficient $C_D$can be obtained by Eq. (12):

$$C_D = \frac{24}{Re_g}(1 + 0.125 Re_g^{0.72}) \tag{12}$$

and the specific surface area per volume of flue gas can be described by:

$$a' = \frac{6L}{D_d \frac{\pi}{4} D_t^2 u_d} \tag{13}$$

2.2.4. *Motion of bubbles forced oxidation process*

In the slurry tank, oxidize air injected in the form of bubbles. With the rising of the bubble, the diameter of the bubble changes as well. As a result, the bubble diameter at time t can be expressed by assuming the ideal gas law:

$$D_{b,t} = \left[\frac{6}{\pi}\left(\sum_{i=1}^{X} \frac{n_{i,t} RT}{P_{b,t}}\right)\right]^{\frac{1}{3}} \tag{14}$$

where, the total pressure inside the bubbles can be obtained by Eq. (15).

$$P_{b,t} = P_{atm} + \rho_l g h + \frac{4\sigma}{D_{b,t}} \tag{15}$$

When t = 0, the $D_{b,0}$ can be written as:

$$D_{b,0} = \left[\frac{6}{\pi}\left(\sum_{i=1}^{X} \frac{n_{i,0} RT}{P_{b,0}}\right)\right]^{\frac{1}{3}} \tag{16}$$

The rising velocity of bubbles can be obtained according to the work of Stokes (1851):

$$u_{b,t} = \frac{1}{6} \frac{g D_{b,t}^2 (\rho_l - \rho_g)}{\mu_l} \frac{1 + \kappa}{2 + 3\kappa} \tag{17}$$

Due to the small viscosity of air ($\kappa = \mu_g/\mu_l \approx 0$) comparing to the slurry, the Eq. (18) can be derived as:

$$u_{b,t} \approx \frac{1}{12} \frac{g D_{b,t}^2 (\rho_l - \rho_g)}{\mu_l} \tag{18}$$

2.2.5. *Calculation process and hybrid modeling method*

In order to calculate the natural oxidation rate η_1 and the utilization rate of oxidize air η_2 according to the model above, the natural oxidation zone and forced oxidation zone are divided into n and m horizontal cells, respectively, as shown in Fig. 1. As a result, the natural oxidation rate η_1 and the utilization rate of oxidize air η_2 can be calculated by the numerical calculation process, and can be described by the following equation:

$$\eta_1 = f_1(E_n, D_d, \quad Q_f, \quad L, H_n, \ldots\ldots) \tag{19}$$

$$\eta_2 = f_2(E_f, D_{b,0}, \quad H_f, \quad \ldots\ldots) \tag{20}$$

According to the mass balance of in the absorber, the absorbed sulfur and the oxidated sulfur in a certain period of time can be calculated by the following equations:

$$S_{ab} = \frac{\Delta t c_{SO_2} Q_f \eta_{SO_2}}{M_{SO_2}} \tag{21}$$

$$S_{ox} = \Delta t \left(\frac{c_{SO_2} Q_f \eta_1 \eta_{SO_2}}{M_{SO_2}} + \frac{2 Q_a \Phi_{O_2} \eta_2}{v_m}\right) \tag{22}$$

where, the η_{SO_2} can be assumed to be 1, due to the high SO_2 removal efficiency of the WFGD system. And, the accumulation (or depletion) of sulfite in a certain period of time can be expressed by the following equation:

$$\Delta c_{S(IV)} = \frac{\Delta t \left(\frac{c_{SO_2} Q_f (1 - \eta_1) \eta_{SO_2}}{M_{SO_2}} - \frac{2 Q_a \Phi_{O_2} \eta_2}{v_m}\right)}{SH_s} \tag{23}$$

In order to avoid the fixed error of the online monitors and improve the accuracy and generality of the model, two correction factors are purposed in order to modify the model. The first correction factor K_1 is the correction for flue gas flow rate and SO_2 concentration. The second factor K_2 is the correction for oxidizing air flow rate. As a result, the rate of

Table 1 – Factors need to be identified in the model.

Category	Symbol	Detail
Characteristic factors	E_n	Enhance factor in the nature oxidation process
	E_f	Enhance factor in the forced oxidation process
	D_d	Diameter of droplets
	$D_{b,0}$	Diameter of bubbles at the bottom of the forced oxidation zone
Correction factors	K_1	Correction for flue gas flow rate and SO_2 concentration
	K_2	Correction of oxidizing air flow rate

accumulation (or depletion) of sulfite in a certain period of time can be expressed by the following equation:

$$\Delta c_{S(IV)} = \frac{K_1 \Delta t \left(\frac{c_{SO_2} Q_f (1 - f_1 (E_n, D_d, \quad Q_f, \quad L, H_n, \ldots\ldots)) \eta_{SO_2}}{M_{SO_2}} - K_2 \frac{2 Q_a \Phi_{O_2} f_2 (E_f, D_{b,0}, \quad H_f, \quad \rho_l, \quad \ldots\ldots)}{v_m} \right)}{S H_f} \tag{24}$$

where, the p_{O_2}, c_{SO_2}, Q_f, L, Q_a, ρ_l and H_f can be measured by the monitors of the DCS of the WFGD system. As a result, these parameters are regard as the input of the model. Also, there are two types of unknown factors in the Eq. (24), namely characteristic factors such as E_n, E_f, D_d, $D_{b,0}$ and correction factors such as K_1, K_2, as shown in Table 1.

According to the model mentioned above, there are 6 factors needed to be identified. The root mean squared error (RMSE) is used as the fitness function, and the identification process can be described by the following optimal problem:

$$\min RMSE(E_n, E_f, D_d, D_b, K_1, K_2) = \sum_{i=0}^{x} \frac{1}{x} (\Delta c_{S(IV)} - \Delta \hat{c}_{S(IV)})^2 \tag{25}$$

Consequently, the identification process is a multi-variable nonlinear programming (NLP) task. And, the PSO algorithm, as a common optimization method for solving nonlinear programming problems, is adopted as the problem solver in this paper. The PSO algorithm will randomly generate numbers of particles in the solution space which is called population. Each particle has a position attribute, which refers to the value of influencing parameters, and a velocity attribute, which refers to the change rate of influencing parameters during iteration. During each iteration, these two attributes of the particles are updated according to their fitness calculated by the objective function using the following equations to make the particle closer to the current optimal position.

$$V_{i,t+1} = \omega V_{i,t} + c_1 r_1 (P_{pbest} - P_{i,t}) + c_2 r_2 (P_{gbest} - P_{i,t}) \tag{26}$$

$$P_{i,t+1} = P_{i,t} + V_{i,t+1} \tag{27}$$

The iteration ends when the accuracy meets the requirement or the iteration number reaches the maximum. The value stored in P_{gbest} at the end of iteration is regarded as the optimal result. The population size and maximum number of iterations are set to be 2000 and 8, respectively. In order to reduce the time consumption on calculation, the parallel computing method is used in this work. The diagrammatic sketch of the construction method of hybrid-model is shown in Fig. 3:

2.3. *Operating optimization strategy*

After obtained the hybrid model of the oxidation system, it is necessary to build the optimization strategy based on the model and calculate the demand for oxidizing air, as shown in Eq. (28):

$$Q_a = \frac{k_1 c_{SO_2} Q_f (1 - \eta_1) \eta_{SO_2} v_m}{k_2 2 \Phi_{O_2} M_{SO_2} \eta_2} \tag{28}$$

In fact, not all oxidation fans are equipped with the variable-frequency drive (VFD), which can realize the continuous adjustment of oxidizing air. Therefore, it is necessary to design the optimization strategy based on the existing equipment. For oxidation fans equipped with VFD, Eq. (28) can be used to calculate the demand of oxidize air and convert it into the frequency of the oxidation fan. For units not equipped with VFD, Eq. (24) can be used to calculate the cumulative amount of sulfite, which can be used as the criterion for switching the oxidation fan on or off , as shown in Fig. 4.

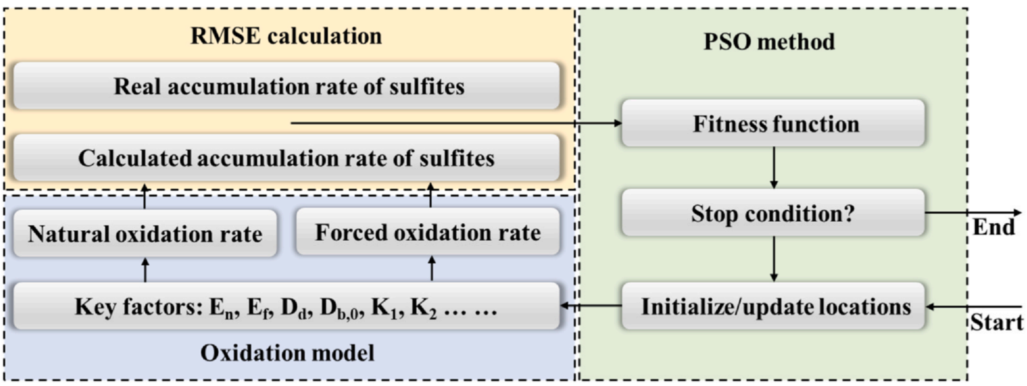

Fig. 3 – Diagrammatic sketch of the construction method of hybrid-model.

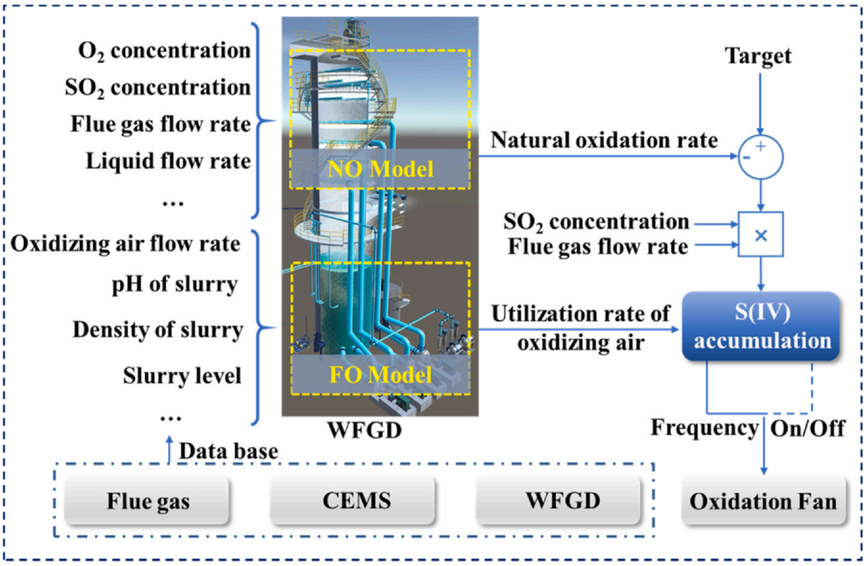

Fig. 4 – Operating optimization strategy of oxidation subsystem.

3. Results and discussion

3.1. Model validation

In order to modify and verify the hybrid model of oxidation process as mentioned above, the slurry in the WFGD system of the 1000 MW unit, as shown in Fig. 5 (a), is sampled and analyzed. The height and diameter of the absorber is 49.55 m and 20.5 m, respectively. The height of the absorption zone is 13.6 m. The distance between layers is 2.7 m. The sulfite concentration in the slurry is measured by iodometric method with a Metrohm 905 Titrando which is shown in Fig. 5 (b). 5 ml of the shaken slurry sample is first added to a beaker. And then add 10 ml of 0.05 mol/L iodine standard titration solution to the beaker. After stirring and reacting in a dark place for 10 min, the leftover iodine is titrated by 0.1 mol/L sodium thiosulfate standard solution. The end point is depended on the ORP. The measured results are used to calculate the parameters of the model. Except for the rate of accumulation (or depletion) of sulfite, all other data are from the supervisory information system (SIS) of the power plant with 10 s interval. The comparison between the predicted value and the measured value is shown in Fig. 5 (c):

As shown in the Fig. 5 (c), after 20 group of tests, the detailed parameters can be obtained, which are shown in the Table 2. The RMSE of the model is 0.149 mol/m^3, indicating that the model can accurately describe the oxidation process in the WFGD system.

3.2. Effect of key factors on the oxidation process

There are many factors that affect the natural oxidation rate and forced oxidation rate in the WFGD system. Among them, the effect of SO_2 concentration in flue gas is intuitive. With the increase of SO_2 concentration, the amount of absorbed SO_2 increase, and both the natural oxidation rate and the forced oxidation rate decrease. In addition, the natural oxidation rate is affected by the diameter of the droplet, the liquid-gas ratio and the height of the natural oxidation zone. While, the forced oxidation rate is affected by the diameter of the bubble, the gas-gas ratio (the ratio of between oxidized air flow rate and flue gas flow rate) and the slurry level in the tank, as shown in Fig. 6:

As shown in Fig. 6 (a), the natural oxidation rate increases with the increase of the liquid-gas ratio and the height of the natural oxidation zone. As the height of the natural oxidation zone increases, the contact time of the droplets with the O_2 in the flue gas is prolonged, thus increasing the natural oxidation rate. As the liquid-to-gas ratio increases, the contact area between the droplets and the flue gas becomes larger, resulting in more O_2 being absorbed, thus increasing the natural oxidation rate. Similarly, as the diameter of droplets

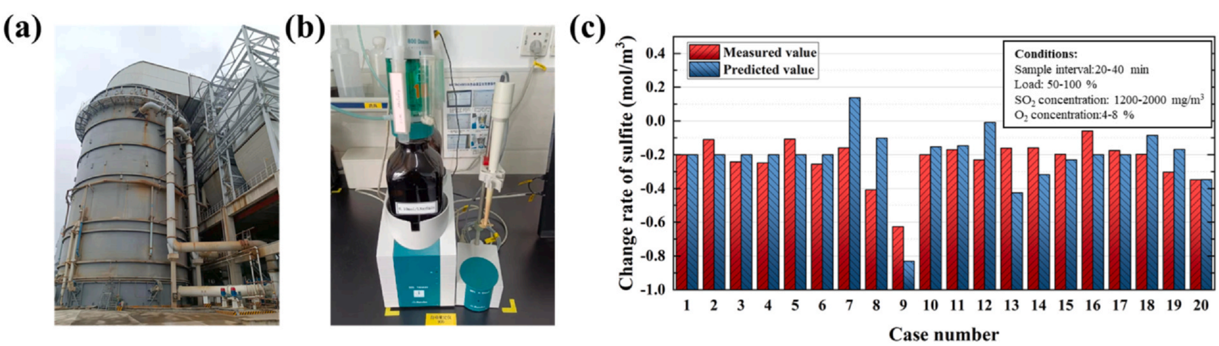

Fig. 5 – *(a)* Photograph of the target WFGD system *(b)* Metrohm 905 Titrando *(c)* Comparison between predicted value and measured value.

Table 2 – Important parameters of the model.

Parameters	Value
E_n	2.389209479
E_f	1.46619443535267
D_d	0.0020817886060659
D_b	0.00140433974954928
K_1	4.286007159
K_2	6.1389579827694

decreases, the specific surface area of the droplet increases significantly so that increasing the natural oxidation rate.

As shown in Fig. 6 **(b)**, the forced oxidation rate increases with the increase of the gas-gas ratio and slurry level. As the slurry level increases, the contact time of the bubbles with the slurry is prolonged, thus increasing the forced oxidation rate. As the gas-gas ratio increases, the contact area between the bubbles and the slurry becomes larger, resulting in more O_2 being absorbed, thus increasing the forced oxidation rate. Similarly, as the diameter of bubbles decreases, the specific surface area of the bubbles increases significantly so that increasing the forced oxidation rate.

3.3. *Operating optimization performance*

Based on the constructed oxidation process prediction model, a real-time optimization system is built on the WFGD system of the 1000 MW unit mentioned above. The oxidation fans can be adjusted by the VFD. Monitors such as the continues emission monitoring system (CEMS) and the flowmeter transmit the measured data to the distributed control system (DCS) system. The object linking and embedding for process control (OPC) server obtain data from DCS and then transmit it to the optimization server and database in real time. The optimization server gives the optimized value every 10 s according to the data from OPC server, and sends it to the database and OPC server. The OPC server writes the optimized value back to the DCS. The structure of the real-time prediction system is shown in Fig. 7 **(a)**.

A field test for long-term operation of the optimization system has been conducted. Taking the operating data of 16 h with large fluctuations in unit load as an example. Actually, before the application of the optimization system, the operation of the oxidation fan is simply divided into two modes. At high load (> 850 MW), the frequency of oxidation fan A and B is 85 Hz and 76 Hz, respectively. And, at medium and low load (< 850 MW), the frequency of oxidation fan A and B is slightly reduced to 75 Hz and 65 Hz. Fig. 7 **(b)** shows the optimized flow rate of oxidizing air under different loads and the comparison of energy consumption before and after optimization.

As shown in Fig. 7 **(b)**, the optimized flow rate of oxidizing air is highly dependent on the unit load. With the increase of load, the flue gas flow rate and the SO_2 concentration both increases, while the O_2 concentration decreases, as shown in Fig. 7 **(c)**, resulting in the decrease of the natural oxidation rate. The average frequency of the oxidation fans at low or middle load decrease for 50 % lower after optimization. The energy consumption of the oxidation fan A and B can be reduced by 23.7 % and 29.6 %, respectively.

3.4. *Application on other WFGD system without VFD*

In order to further verify the optimization method, the application study is also carried out on the WFGD system of 220 t/h and 130 t/h circulating fluidized bed (CFB) units. Since the oxidation fans of these two WFGD systems are not equipped with VFD. Therefore, the oxidation subsystem is optimized by on/off adjustment. The cumulative amount of sulfite is calculated by the Eq. (24). When the calculated concentration of the sulfite reaches a certain value (5.8 mol/m^3 in the practice), the oxidation fan will be turned on. In order to ensure the safety of the WFGD system, an upper limit of 3 h is set for the shutdown time of the oxidation fans. At the same time, due to the irregular discharge of slurry during the daytime, in order to ensure the dewatering performance of the discharged gypsum, the optimization system will not be applied during the daytime. Since the shutdown of the oxidation fan may affect the contents of the slurry, thereby affecting the safe operation of the WFGD, the

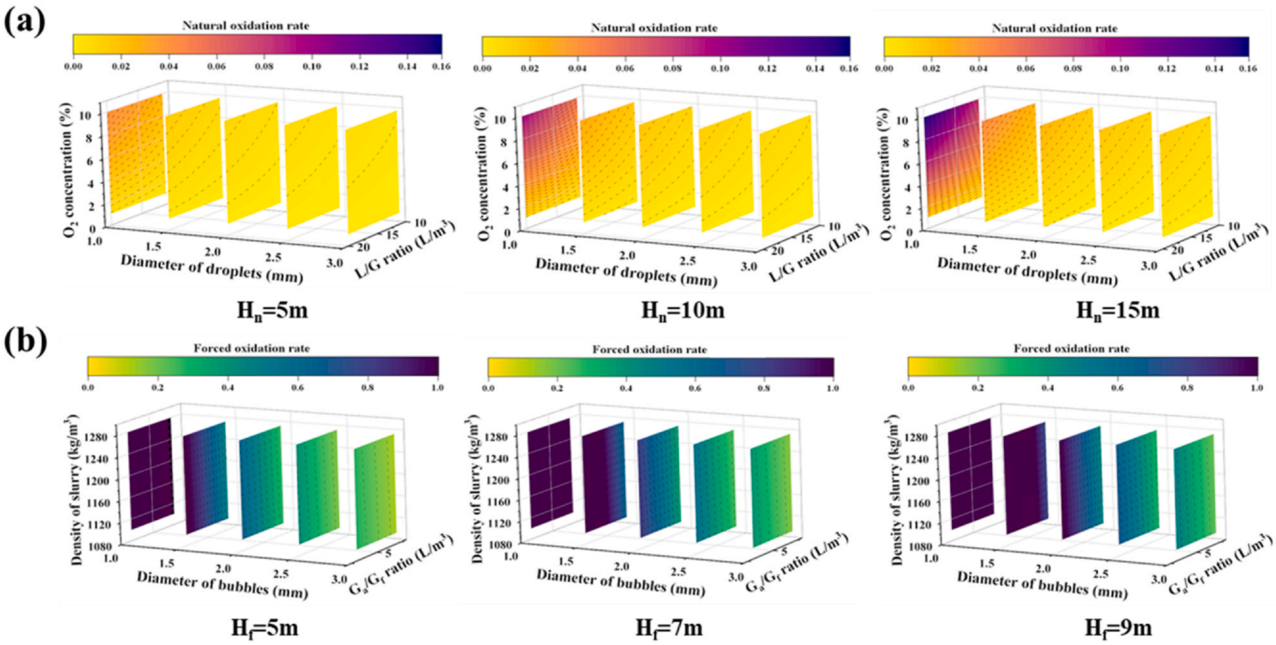

Fig. 6 – The effects of important factors on *(a)* nature oxidation rate and *(b)* forced oxidation rate.

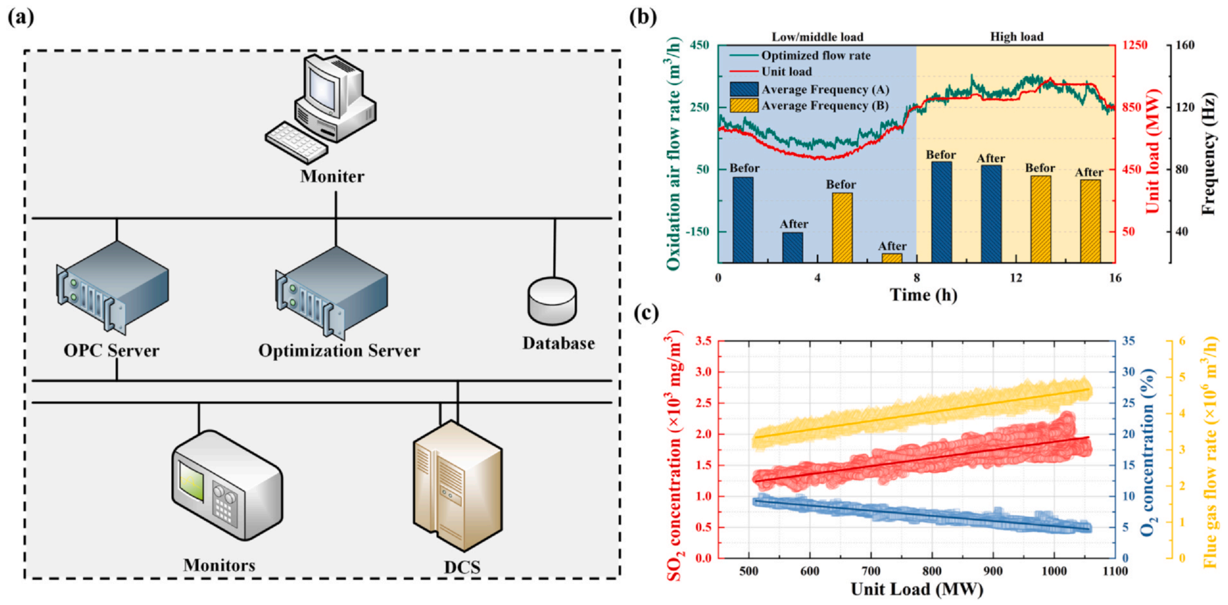

Fig. 7 – (a) The structure of the real-time optimization system. (b) Results of the optimization system. (c) Key parameters under different load.

sulfite content, pH value, and dissolved oxygen content are monitored by slurry sampling during the commissioning period. The interval of sampling is 20 min. Fig. 8 shows the changes of key parameters in the slurry within 1 cycle (the time between the current shutdown of the oxidation fan and the next shutdown).

As shown in Fig. 8, for the 130 t/h unit, when the oxidation fan is turned off, the dissolved oxygen in the slurry is rapidly consumed, from 5 mg/L to 0.5 mg/L, and the pH value of the slurry will drop slightly, due to the accumulation of sulfite. The sulfite concentration reached the highest 6.1 mol/m^3 before the fan is switched on. For the 220 t/h unit, after turning off the oxidation fan for 3 h, the concentration of sulfite gradually increased from 2.6 mol/m^3 to the highest 5.4 mol/m^3. The results show that there will be a small amount of sulfite accumulating in the slurry during the shutdown period of the oxidation fan, and will not affect the desulfurization process. After one cycle, the sulfite concentration can eventually drop to the sulfite concentration before the cycle start, which will not affect the quality of gypsum.

Fig. 9 compares the energy consumption for one week before and after the optimization system is put into operation. For the 130 t/h unit, the average operating power of the oxidation fan is reduced from 36 kW to 25 kW, and the energy

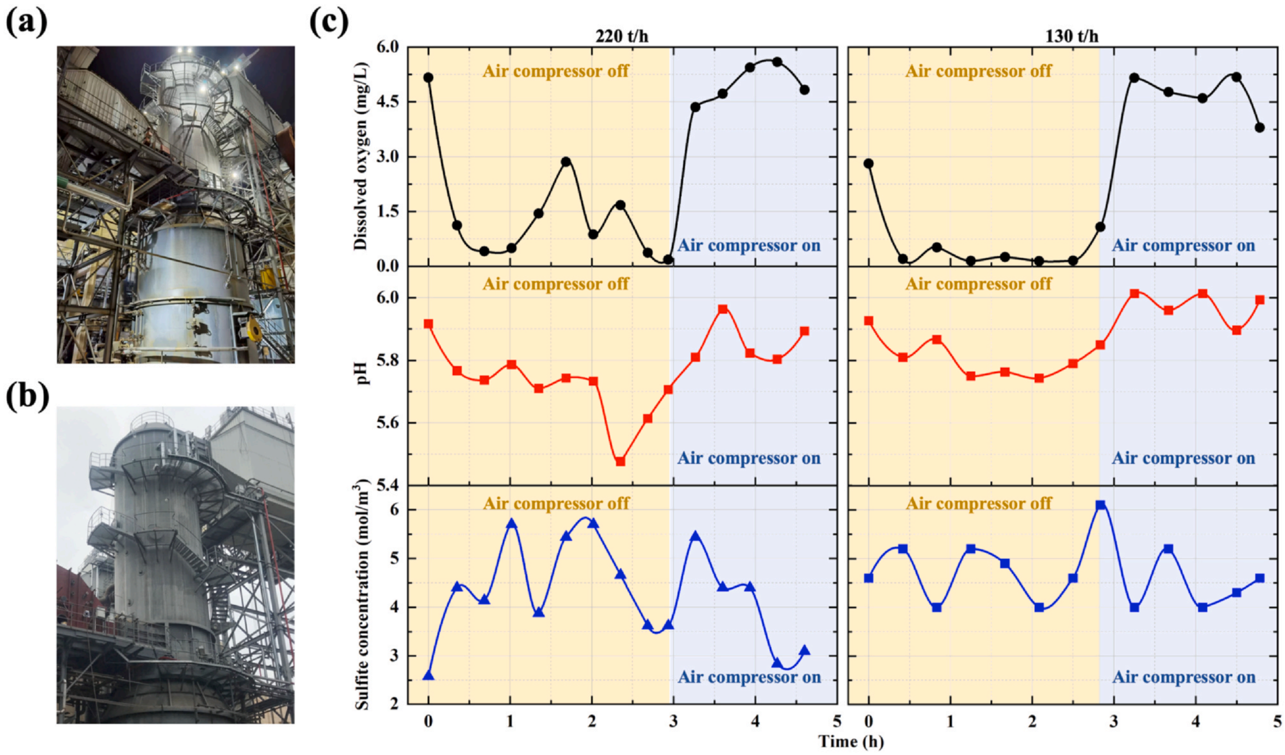

Fig. 8 – Photographs of WFGD system of (a) 220 t/h and (b)130 t/h CFB units and (c) results of the optimization system.

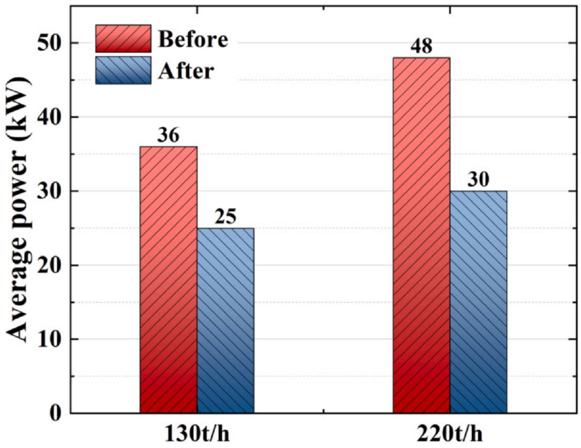

Fig. 9 – Comparison of the energy consumption.

consumption is reduced by 30.6 %. For the 220 t/h unit, the average power of the oxidation fan is reduced from 48 kW to 30 kW, and the energy consumption is reduced by 37.5 %.

4. Conclusion

In this paper, a hybrid modeling and operating optimization method of oxidation process of WFGD system is proposed, verified and applied on the WFGD system of a typical 1000 MW unit. The model is verified based on the experiment. The RMSE of the model is 0.149 mol/m^3, indicating that the model can accurately describe the oxidation process in the WFGD system. The influence of important parameters such as the diameter of droplets or bubbles, the liquid-gas ratio or the gas-gas ratio and the height of the natural oxidation zone or the slurry level on natural oxidation rate and forced oxidation rate are further explored. Based on the constructed oxidation process prediction model, a real-time optimization system is built on the WFGD system of the 1000 MW unit mentioned above. Taking the operating data of 16 h with large fluctuations in unit load as an example. The average frequency of the oxidation fans at low or middle load are reduced by 50 % after optimization. The energy consumption of the oxidation fan A and B can be reduced by 23.7 % and 29.6 %, respectively. Furthermore, field tests are also carried out on the WFGD systems of 130 t/h and 220 t/h circulating fluidized bed (CFB) units. The energy consumption can be reduced by 30.6 % and 37.5 %, respectively. The accumulation of sulfite will not affect the desulfurization process and the quality of gypsum. The results will be helpful to reduce the auxiliary power consumption and additional CO_2 emission of WFGD.

Declaration of Competing Interest

The authors declare that they have no known competing financial interests or personal relationships that could have appeared to influence the work reported in this paper.

Acknowledgement

This work is supported by National Key R&D Program of China (No. 2020YFB0606203-4) and Development Plan of Shandong Province of China (2020CXGC011401).

References

Abel, D.W., et al., 2019. Air quality-related health benefits of energy efficiency in the United States. Environ. Sci. Technol. 53 (7), 3987–3998.

Banerjee, S., Scott, D.S., Rhodes, E., 1968. Mass transfer to falling wavy liquid films in turbulent flow. Ind. Eng. Chem. Fundam. 7 (1), 22–27.

Chang, C.J., et al., 2019. Employing a fuzzy-based grey modeling procedure to forecast China's sulfur dioxide emissions. Int. J. Environ. Res. Public Health 16 (14), 10.

Chen, M., Deng, X., He, F., 2017. Study on the kinetics of S(IV) oxidation in the basic aluminum sulfate wet flue gas desulfurization process. RSC Adv. 7 (62), 39341–39348.

Chen, T.-L., Chen, Y.-H., Chiang, P.-C., 2020. Enhanced performance on simultaneous removal of NO_x-SO_2-CO_2 using a high-gravity rotating packed bed and alkaline wastes towards green process intensification. Chem. Eng. J. 393, 124678.

Ministry of Ecology and Environment, The People's Republic of China, 2022. Annual Statistic Report on Ecologyand Environment in China 2020. Ministry of Ecologyand Environment of the People's Republic of China, Beijing.

China, N.B.o.S.o., 2021. China Statistical Yearbook. National Bureau of Statistics of China.

Córdoba, P., 2015. Status of flue gas desulphurisation (FGD) systems from coal-fired power plants: overview of the physic-chemical control processes of wet limestone FGDs. Fuel 144, 274–286.

Flagiello, D., et al., 2018. Experimental and modelling analysis of seawater scrubbers for sulphur dioxide removal from flue-gas. Fuel 214, 254–263.

Fuller, E.N., Schettler, P.D., Giddings, J.C., 1966. New method for prediction of binary gas-phase diffusion coefficients. Ind. Eng. Chem. 58 (5), 18–27.

Gerbec, M., Stergaršek, A., Kocjančič, R., 1995. Simulation model of wet flue gas desulphurization plant. Comput. Chem. Eng. 19, 283–286.

Gong, Y., Yang, Z.-G., 2018. Corrosion evaluation of one wet desulfurization equipment – flue gas desulfurization unit. Fuel Process. Technol. 181, 279–293.

Gu, S., et al., 2020. Dissolution reactivity and kinetics of low-grade limestone for wet flue gas desulfurization. Ind. Eng. Chem. Res. 59 (32), 14242–14251.

Guo, Lin, et al., 2017. Reaction kinetics of non-catalyzed jet aeration oxidation of magnesium sulfite. Chem. Eng. J., S1385894717313165.

Guo, Y., et al., 2018. Hybrid modeling scheme for PM concentration prediction of electrostatic precipitators. Powder Technol. 340, 163–172.

Guo, Y., et al., 2019. Modeling and optimization of wet flue gas desulfurization system based on a hybrid modeling method. J. Air Waste Manag Assoc. 69 (5), 565–575.

Jia, Yong, et al., 2010. Kinetics of oxidation of total sulfite in the ammonia-based wet flue gas desulfurization process. Chem. Eng. J. 164.1, 132–138.

Kallinikos, L.E., et al., 2010. Simulation of the operation of an industrial wet flue gas desulfurization system. Fuel Process. Technol. 91 (12), 1794–1802.

Lamont, J.C., Scott, D.S., 1970. An eddy cell model of mass transfer into the surface of a turbulent liquid. AIChE J. 16 (4), 513–519.

Lawson, John M., et al., 2019. Direct assessment of Kolmogorov's first refined similarity hypothesis. Phys. Rev. Fluids.

Lee, M.H., 2000. Fick's law, Green-Kubo formula, and Heisenberg's equation of motion. Phys. Rev. Lett. 85.12, 2422.

Li, X., et al., 2022. Summary of research progress on industrial flue gas desulfurization technology. Sep. Purif. Technol. 281, 119849.

Liu, C., et al., 2021. Process optimization of S (IV) oxidation in flue gas desulfurization scrubbers. Process Saf. Environ. Prot. 149, 610–618.

Liu, C., et al., 2022. Experimental study and modified modeling on effect of SO_2 on CO_2 absorption using amine solution. Chem. Eng. J. 448, 137751.

Liu, Q., et al., 2017. Modeling and prediction for the oxidation efficiency of magnesium sulfite in aeration tank of magnesium-based seawater exhaust gas clean system. Proc. Inst. Mech. Eng. Part M: J. Eng. Marit. Environ. 233 (1), 164–173.
Ma, S., et al., 2019. Factors affecting slurry oxidation in a wet flue gas desulfurization process. J. Environ. Eng. 145 (10), 04019058.
Michalski, J.A., 2000. Aerodynamic characteristics of flue gas desulfurization spray towerspolydispersity consideration. Ind. Eng. Chem. Res. 39 (9), 3314–3324.
National Development and Reform Commission of PRC, M.o.E.P. o.P., National Energy Administration of PRC, 2014. The upgrade and transformation action plan for coal-fired power energy saving and emission reduction (2014–2020).
Othmer, D.F., Thakar, M.S., 1953. Correlating diffusion coefficient in liquids. Ind. Eng. Chem. 45 (3), 589–593.
Pandey, R.A., et al., 2005. Flue gas desulfurization: physicochemical and biotechnological approaches. Crit. Rev. Environ. Sci. Technol. 35 (6), 571–622.
Pyshyev, S., et al., 2017. State of the art in the field of emission reduction of sulphur dioxide produced during coal combustion. Crit. Rev. Environ. Sci. Technol. 47 (24), 2387–2414.
Sander, R., 2015. Compilation of Henry's law constants (version 4.0) for water as solvent. Atmos. Chem. Phys. 15, 4399–4981.
Shen, J., et al., 2019. Atmospheric emission inventory of SO3 from coal-fired power plants in China in the period 2009–2014. Atmos. Environ. 197, 14–21.
Shen, Z., et al., 2012. Kinetics and mechanism of sulfite oxidation in the magnesium-based wet flue gas desulfurization process. Ind. Eng. Chem. Res. 51 (11), 4192–4198.
Smith, S.J., et al., 2011. Anthropogenic sulfur dioxide emissions: 1850–2005. Atmos. Chem. Phys. 11 (3), 1101–1116.
Srivastava, R.K., Jozewicz, W., 2001. Flue gas desulfurization: the state of the art. J. Air Waste Manag. Assoc. 51 (12), 1676–1688.
Srivastava, R.K., Jozewicz, W., Singer, C., 2001. SO2 scrubbing technologies: a review. Environ. Prog. 20 (4), 219–228.
Stokes, G.G., 1851. On the Effect of the Internal Friction of Fluids on the Motion of Pendulums. Pitt Press Cambridge, Cambridge.
Wang, H., et al., 2019. A critical review on the method of simultaneous removal of multi-air-pollutant in flue gas. Chem. Eng. J. 378, 122155.
Wang, X., et al., 2019. A unit-based emission inventory of SO_2, NO_x and PM for the Chinese iron and steel industry from 2010 to 2015. Sci. Total Environ. 676, 18–30.
Yi, Z., et al., 2011. Wet flue gas desulfurization using a physical mixture of limestone and lime for energy savings, In: Proceedings of the 2011 International Symposium on Water Resource and Environmental Protection.
Zhang, J., Zheng, C., Zhang, Y., et al., 2016. Experimental investigation of sulfite oxidation enhancement in a micro-pore aeration system. RSC Adv. 10, 1039.
Zhao, Z., et al., 2022. Simulation of SO_2 removal process from marine exhaust gas by hybrid exhaust gas cleaning systems (EGCS) using seawater and magnesium-based absorbent. Sep. Purif. Technol. 287, 120557.
Zhao, Z.Y., et al., 2021. Simulation of SO_2 absorption and performance enhancement of wet flue gas desulfurization system. Process Saf. Environ. Prot. 150, 453–463.
Zheng, C., et al., 2014. Nitrogen oxide absorption and nitrite/nitrate formation in limestone slurry for WFGD system. Appl. Energy 129, 187–194.
Zheng, C., et al., 2019. Formation, transformation, measurement, and control of SO_3 in coal-fired power plants. Fuel 241, 327–346.
Zhou, H., Guo, W.S., Zhu, Y.F., et al., 2017. Flow distribution characteristics of low-pressure high-flux spiral nozzles. J. Chin. Soc. Power Eng. 37 (07), 577–583.
Zou, R., et al., 2020. Modeling study of selenium migration behavior in wet flue gas desulfurization spray towers. Environ. Sci. Technol. 54 (24), 16128–16137.